

Synthetic Muon-Gravity Study at Redondo Peak, Valles Caldera, New Mexico

Brady Spears

Abstract

Muon tomography presents an innovative approach to probing subsurface density structures, especially when combined with other geophysical data sets. In particular, gravity and muon range data both relate linearly to density and provide vastly different spatial sensitivities, allowing either dataset to compensate for the other's shortcomings. Here, we computationally explore and model an optimized scenario for performing a multi-detector, joint muon-gravity survey at a lava dome structure known as Redondo Peak in the Valles Caldera, New Mexico. We utilize topographic information to create a finite-element forward model in which we generate muon ranges and synthetic gravity measurements before introducing density perturbations and performing the inversion. Our results detail that a three-detector muon survey constrained to roads surrounding the peak would be operating at very high polar angles ($\theta > 80^\circ$) and that several trajectories passing through the peak would exhibit range values that are simply too large for energetic muons to penetrate. Despite these adversarial factors, our joint-inversion scheme is able to accurately resolve the principal subsurface density anomalies introduced in the forward calculation.



Department of Physics and Astronomy
Under the supervision of Dr. Mousumi Roy
University of New Mexico
May 2020

1 Introduction

Density mapping proves its application in a variety of earth science problems. Arguably the most pertinent of these resides in mitigating risk associated with volcanic hazards. In locations where magmatic sources are active and pose risk to a local population, the ability to directly detect and monitor dynamic density behavior associated with subsurface magmas (Poland and Carbone, 2014), volatile fluid in hydrothermal vents (LeGonidec et al., 2019), or infiltrating rain water (Farquharson and Amelung, 2020) is the first step in potentially predicting disaster before its manifestation at the surface (Tanaka et al. 2007, 2010, 2015).

There exist a number of geophysical techniques aimed at resolving subsurface density features. These include most notably seismic, gravity, and cosmic-ray muon tomography. Several prior studies have proven the applicability of these techniques in resolving subsurface densities as stand-alone practices (Burger et al., 2006), however each carries its own inherent limitations. Seismic wave speed inversion, for example, requires inferences to be made about the subsurface itself, like thermal structure, composition, and porosity; all of which can affect the resolved density values. Gravity is inherently non-unique, requiring strong *a priori* information about the density structure of a study area to be included in an inversion model. Muon tomography is the most passive and sensitive of the three methods, but is ill-posed, as it is only sensitive to model parameters along a given muon’s path through rock. Standing alone, each technique features limitation, but a joint approach aimed at combining gravity data with one or more of these techniques can mitigate the non-uniqueness associated with gravity and constrain the inversion with limited information of the subsurface density structure available.

For this particular study, we focus on muon tomography and gravity - two techniques that, unlike seismic surveys, relate linearly to density. Gravity relates familiarly to density by Newton’s law of gravitation. Muon tomography, however, is more novel. Cosmic-ray muons are generated by the decay of pions and kaons in the upper atmosphere. Muons are comparable to electrons, but feature about 200 times the mass of an electron, which allows them to more readily pass through matter (Alvarez et al., 1970). Although muons are unstable and have decay lifetimes on the order of 10^{-6} s, their relativistic nature allows them to reach into Earth’s surface before they inevitably decay. The attenuation of muons through matter is well-understood (Leo, 1987), and is a function of the integrated density-length, or range, along a muon’s path (Groom et al. 2001). Although gravity measurements are sensitive to all elements in a model, gravity’s sensitivity falls off as an inverse-square law. This is in contrast to muon measurements, which feature a much higher sensitivity but are only sensitive to those elements in the model through which muons pass. The non-unique behavior of gravity inversion is therefore constrained by the higher-sensitivity muon measurements, and the expanse of gravity measurements through the entire model combats the ill-posed muon measurements (Jourde et al., 2014; Nishiyama et al., 2014).

Building on the work of Cosburn et al. (2019), where a joint-inversion of gravity and muon data was investigated to characterize the density structure of a well-understood area, we investigate both the feasibility and results of a similar joint muon-gravity study at Redondo Peak in the Valles Caldera, New Mexico. Although Redondo Peak is not volcanically active, it presents an ideal field study area for its high prominence, association with magmatic

processes, and its logging trails, which surround the peak on all sides.

We will be investigating our study computationally by assuming a field-deployable and pointable detector. In this study, we deployed three detectors in our survey area that were constrained to easily-accessible logging roads and separated at roughly 120° about the apex of Redondo Peak. We also generated synthetic gravity measurements for 121 uniformly-spaced, gridded gravity measurement stations. The goal of this study is to create an idealized experimental setup in regards to the geometry of the study area, and investigate the results of such a setup.

2 Forward Method

Our model is discretized from topographic information of Redondo Peak and its immediate surrounding area (Fig. 2). GIS road point data has also been obtained for the region and corresponds to the various roads and logging trails that surround the Peak (Fig. 1). For the purposes of our study, we constrained the detectors to locations on these roads, a realistic expectation of performing the study in the field, assuming that the detector must be deployed in a relatively accessible area.

2.1 Density Structure

We are concerned with potentially monitoring hydrologic signals, as it has been suggested that anomalously high precipitation can influence shallow volcanic processes (Matthews and Barclay, 2004). While it is highly unlikely that volcanic activity will be induced within the Valles Caldera, a high heat flux impacting infiltrated water can present hydrothermal dangers to the surrounding area. To roughly mimic the effects of infiltrated water as a long-term static density anomaly, we assign every element in the model a base density, $\rho_{base} = 2700$ kg/m³ and subsequently perturb every element that falls within 50 to 150 m of the surface. This very loosely resembles a 100 m thick water table that conforms to the topography of the peak. The magnitude of the perturbation for model elements that meet the depth criterion is calculated as:

$$\rho_{pert} = \rho_{base} + \alpha\rho_{base}$$

where α represents some fraction. We set this value to 5%, corresponding to an increase of 135 kg/m³ for elements within the depth boundaries. This 135 kg/m³ value was chosen as it represents the minimum density change that would be resolvable in the field for the introduced geometry by a common Scintrex CG-5 gravimeter, which has a sensitivity of about 0.05 mgals.

This phenomenon can be thought of geologically as the infiltration of rainwater into subsurface voids and the subsequent precipitation of minerals derived from that rainwater in those voids, resulting in a higher-than-average density anomaly at a certain hydrologic penetration depth (Fig. 3). The deposited minerals in pore space of the base rock correspond to a positive anomaly, but a negative anomaly could also be postulated if the rainwater acted corrosively to increase the volume of void space at the penetrating depth.

2.2 Optimization of Detector Locations

It is well-understood that the penetrating depth of muons decreases dramatically at polar angles near horizontal (Nagamine et al., 1995). Given the topographic geometry and the height of the peak, our study is operating at very high polar angles, so it is desirable to optimize our detector locations so that muons are encountering very little rock along their path, ensuring that as many muons can penetrate as possible.

We first accomplished this optimization by selecting a reference point, essentially a common point at which all detectors were pointed at. In our case, we set this reference point to lie at a depth of 50 m directly below the peak. We drew a single central trajectory from each road point through the reference point and exiting the topography, allowing us to estimate the path length through the mountain. We then selected the road point with the shortest rock path length as the location for our first detector and then derived the other two detectors' locations by constraining a subset of road points that were azimuthally separated from the first detector about the reference point by $\pm 120^\circ$. A subset of acceptable road points were selected that deviated only slightly from this ideal separation value, and the road point of that subset that featured the smallest path length through the topography was ultimately selected as the location for the next detector (Fig. 2).

2.3 Range Values

Given an introduced density structure and locations of our detectors, we then populated each detector with 1600 total trajectories, arranged in a 40-by-40 grid. For a j^{th} trajectory, the range value, R_j is calculated as:

$$R_j = \sum_i L_{ij} \rho_i$$

where L_{ij} is the path length through the i^{th} model element for the j^{th} trajectory, and ρ_i is the density of the associated model element. From each detector, we were able to generate the synthetic range plots shown in Fig. 4.

Upon generation of each trajectory's range, we consulted empirical evidence to identify the maximum energy that ambient muons would be observed at. This value of 4.7 TeV corresponded to a maximum range through rock of $5.24e6 \text{ kg/m}^2$ (Groom et al., 2001). Any trajectories within our model that featured ranges above this threshold were not included in the inversion, and any trajectories that did not intersect the mountain at all were not included in the inversion.

2.4 Gravity

Using 121 gravity stations placed in gridded format over the topography, we synthetically generated the expected downward component of the gravitational acceleration vector as:

$$g_{i,z} = \sum_i G_{ij} \rho_i$$

where G_{ij} is generated from a solution for the gravity effect of a rectangular prism put forth by Nagy et al. (2000). Locations of our gravity stations and the resultant gravity values are shown in Fig. 5.

3 Joint Inversion

We applied a Bayesian joint inversion technique with the synthetically modeled gravity-muon data sets. Using the interaction kernels, L_{ij} and G_{ij} defined above, we constructed the basis of our inversion as:

$$\mathbf{d} = \sum_{i=1} \begin{bmatrix} G_{ij} \\ L_{ij} \end{bmatrix} \rho_i = \sum_{i=1} J_{ij} \rho_i = \mathbf{J} \rho$$

This system is inverted for the model parameter, ρ , by:

$$\rho = \rho_0 + (\mathbf{J}^T \mathbf{C}_d^{-1} \mathbf{J} + \mathbf{C}_m^{-1})^{-1} \mathbf{J}^T \mathbf{C}_d^{-1} (\mathbf{d}_{obs} - \mathbf{d}_{pred})$$

where ρ_0 is the *a priori* density model, \mathbf{C}_d is the model covariance, and \mathbf{C}_m is the model covariance. The inversion was solved iteratively, and aimed at minimizing the L2-norm of $\rho_0 - \rho$ (Tarantola, 2005).

Any variability in ρ is constrained by defining \mathbf{C}_m as an exponential and isotropic smoothing function, parameterized by the correlation length, λ . For a pair of elements (i, k) , \mathbf{C}_m is defined as:

$$C_{m,ik} = \sigma_\rho^2 \exp\left\{\frac{-r_{ik}}{\lambda}\right\}$$

where r_{ik} is the distance between voxels i and k and σ_ρ is simply the standard deviation of the model's density. All muon and gravity measurements were assumed to be uncorrelated, so \mathbf{C}_d is taken to be a diagonal matrix, sized by the number of gravity measurements and the number of trajectories whose range values are nonzero and are under a maximum threshold derived from the maximum energy seen in atmospheric muons.

4 Results and Conclusion

We present an inversion result given a constant density prior model input. Our model inversion utilized 3 muon detectors viewing Redondo Peak from three different sides and 121 gravity stations arranged as a grid sitting atop the topography. We also defined hyperparameters σ_ρ , λ , and ρ_0 based on true values introduced in the forward model, ensuring that the inversion result is the most accurate reconstruction possible. It is important to note that in a field setting, these hyperparameters would likely not be previously known and would rather have to be found via grid search methods as was done in Cosburn et al. (2019). Our recovered density structure is shown in Fig. 6.

In locations of the mountain constrained by muon measurements, specifically the top of the peak, the correct density structure is roughly reconstructed from the inversion scheme. In those areas not constrained by muon measurements, gravity exists as the singular data

set, and conjures its inherently non-unique behavior, failing to resolve the density anomaly below the surface. The juxtaposed results further prove the complementary nature of these two spatially-sensitive measurements (Jourde et al., 2014).

A number of limitations have been identified in the study and are specifically related to the operation of all three detectors at polar angles greater than 80° . While it is possible to observe muons near the horizon, muon flux is drastically lower than at smaller polar angles (Nagamine et al., 1995). Additionally, as the path length of a muon's trajectory through rock increases with depth below the Peak, the muon requires more energy to penetrate and deposit on the detector. This presents an issue as muons at high polar angles are generally not equipped with the energy necessary to pass through such large range values. We recognize that in the field, the ability to actually collect the muon measurements will present a range of issues, but we cite these as inherent and unavoidable limitations to the study.

We expand on the work of Cosburn et al. (2019), applying an inversion scheme using multiple, pointable muon detectors and surface gravity measurements to constrain the static 3-Dimensional density structure of Redondo Peak. In future endeavours, the study will prove its worth as the study transitions from synthetic tests to field tests. This study shows that a synthetic joint inversion of muon and gravity data is a crucial first step toward optimizing a field campaign with limited resources and limited accessibility around a target volcanic edifice.

5 Acknowledgements

I would like to extend my gratitude to Dr. Mousumi Roy and Katherine Cosburn for their guidance, patience, and support with all aspects of my research and academics over the years. Thank you also to the other members of my research group, Vincent Enders and Petra Pierce, for their discussions, advice, and questions on this work. I would also like to thank the Rayburn Reaching Up Fund and the Harry and Mabel F. Leonard Fellowship for their contributions to my work.

References

- [1] Alvarez, L. W., Anderson, J. A., El Bedwei, F., Burkhard, J., Fakhry, A., Girgis, A., Goneid, A., Hassan, F., Iverson, D., Lynch, G., Miligy, Z., Moussa, A. H., Sharkawi, M., Yazolino, L. (1970). Search for Hidden Chambers in the Pyramids. *Science*, 167, 832-839.
- [2] Burger, H. R., Sheehan, A. F., Jones, C. H. (2006). *Introduction to Applied Geophysics: Exploring the Shallow Subsurface*, W. W. Norton Publishers.
- [3] Cosburn, K., Roy, M., Guardincerri, E., Rowe, C. (2019). Joint inversion of gravity with cosmic ray muon data at a well-characterized site for shallow subsurface density prediction. *Geophys. J. Int.*, 217, 1988-2002.
- [4] Farquharson, J. I., Amelung, F. (2020). Extreme rainfall triggered the 2018 rift eruption at Kilauea Volcano. *Nature*, 580, 491-495.

- [5] Groom, D. E., Mokhov, N.V., Striganov, S. I. 2001. Muon stopping power and range tables 10 MeV-100 Tev, *At. Data Nucl. Data Tables*, 78(2), 183-356.
- [6] Jourde, K., Gibert, D., Marteau, J. (2014). Joint inversion of muon tomography and gravimetry - a resolving kernel approach, *Geosci. Instrum. Method. Data Syst. Discuss.*, 5, 83-116.
- [7] LeGonidec Y., Rosas-Carbajal, M., de Bremond d’Ars, J., Carlus, B., Ianigro, J. C., Kergosien, B., Marteau, J., Gibert, D. (2019). Abrupt changes of hydrothermal activity in a lava dome detected by combined seismic and muon monitoring. *Sci Rep*, 9, 3079.
- [8] Leo, W., 1987. *Techniques for Nuclear and Particle Physics Experiments*, Springer.
- [9] Matthews, A. J., Barclay, J. A. (2004). A thermodynamical model for rainfall-triggered dome collapse. *Geophys. Res. Lett.*, 31, L05614.
- [10] Nagamine, K., Iwasaki, M., Shimomura, K., Ishida, K. (1995). Method of porbing inner-structure of geophysical substance with horizontal cosmic-ray muons and possible application to volcanic eruption prediction. *Nuclear Instruments and Methods in Physics Research Section A: Accelerators, Spectrometers, Detectors and Associated Equipment*, 356(2), 585-595.
- [11] Nagy, D., Papp, G., Benedek, J. (2000). The gravitational potential and its derivatives for the prism, *J. Geod.*, 74(7-8), 552-560.
- [12] Nishiyama, R., Tanaka, Y., Okubo, S., Oshima, H., Tanaka, H. K., Maekawa, T. (2014). Integrated processing of muon radiography and gravity anomaly data toward the realization of high-resolution 3-D density structural analysis of volcanoes: case study of Showa-Shhinzan lava dome, Usu, Japan. *J. geophys. Res.*, 119(1), 699-710.
- [13] Poland, M. P., Carbone, D. (2016). Insights into shallow magmatic processes at Kilauea Volcano, Hawai’i, from a multiyear continuous gravity time series. *J. Geophys. Res. Solid Earth*, 121, 5477-5492.
- [14] Tarantola, A. (2005). *Inverse Problem Theory and Methods for Model Parameter Estimation*. Society for Industrial and Applied Mathematics.
- [15] Tanaka, H. K. M., Nakano, T., Takahashi, S., Yoshida, J., Takeo, M., Oikawa, J., et al. (2007). High resolution imaging in the inhomogeneous crust with cosmic ray muon radiography: The density structure below the volcanic crater floor of Mt. Asama, Japan. *Earth and Planetary Science Letters*, 263, 104-113.
- [16] Tanaka, H. K. M., Taira, H., Uchida, T., Tanaka, M., Takeo, M., Ohminato, T., et al. (2010). Three-dimensional computational axial tomography scan of a volcano with cosmic ray muon radiography. *Journal of Geophysical Research*, 115, B12332. doi: <https://doi.org/10.1029/2010JB007677>
- [17] Tanaka, H. K. M. (2015). Muographic mapping of the subsurface density structures in Miura, Boso and Izu peninsulas, Japan. *Scientific Reports*, 5, 8305.

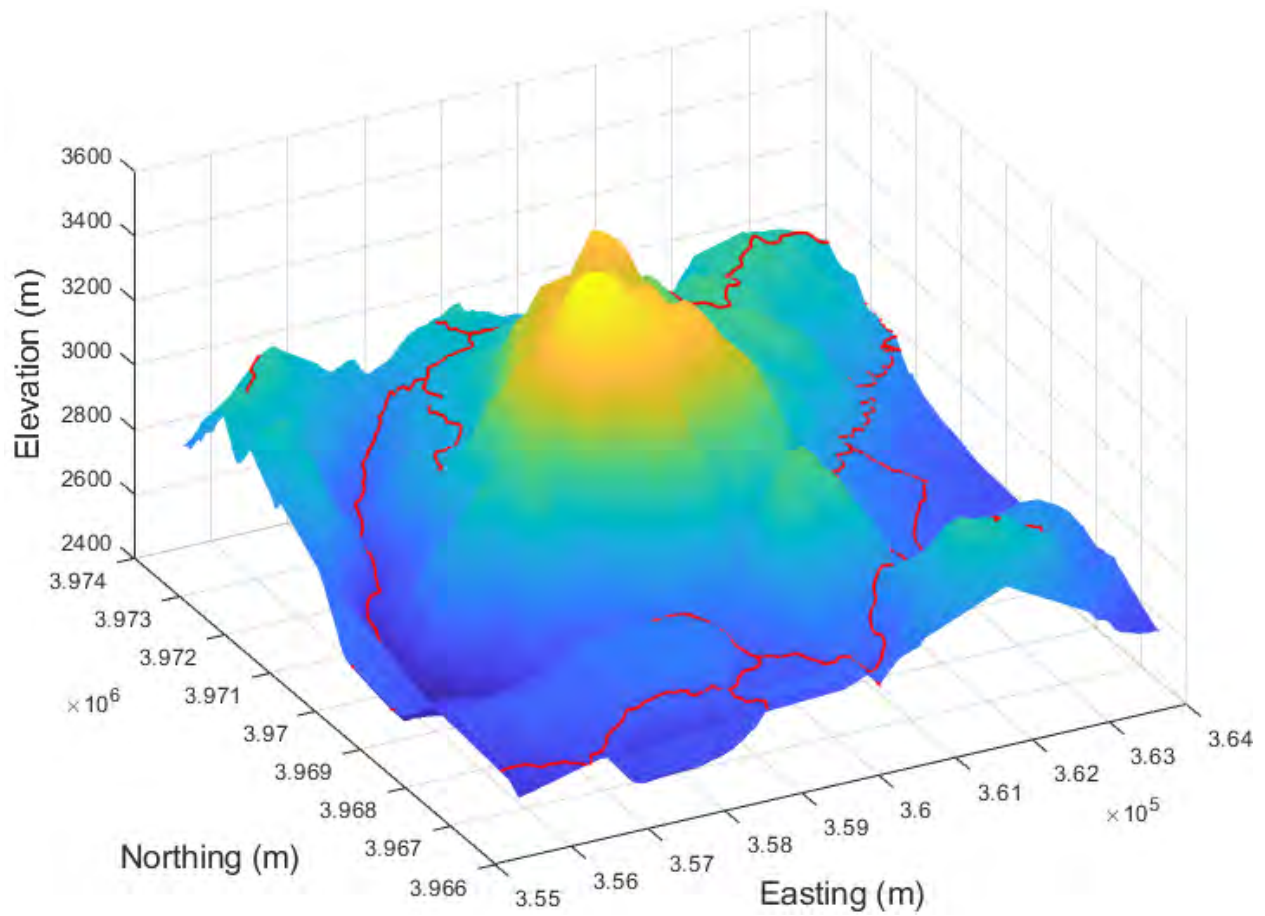


Figure 1: Interpolated high-resolution LIDAR topography of Redondo Peak and the surrounding study area obtained from OpenTopography.org. Redondo Peak is the highest point of this rendered surface. Potential detector deployment locations, also known as GIS road point data, is plotted in red and represent the various logging trails that surround the Peak on all sides.

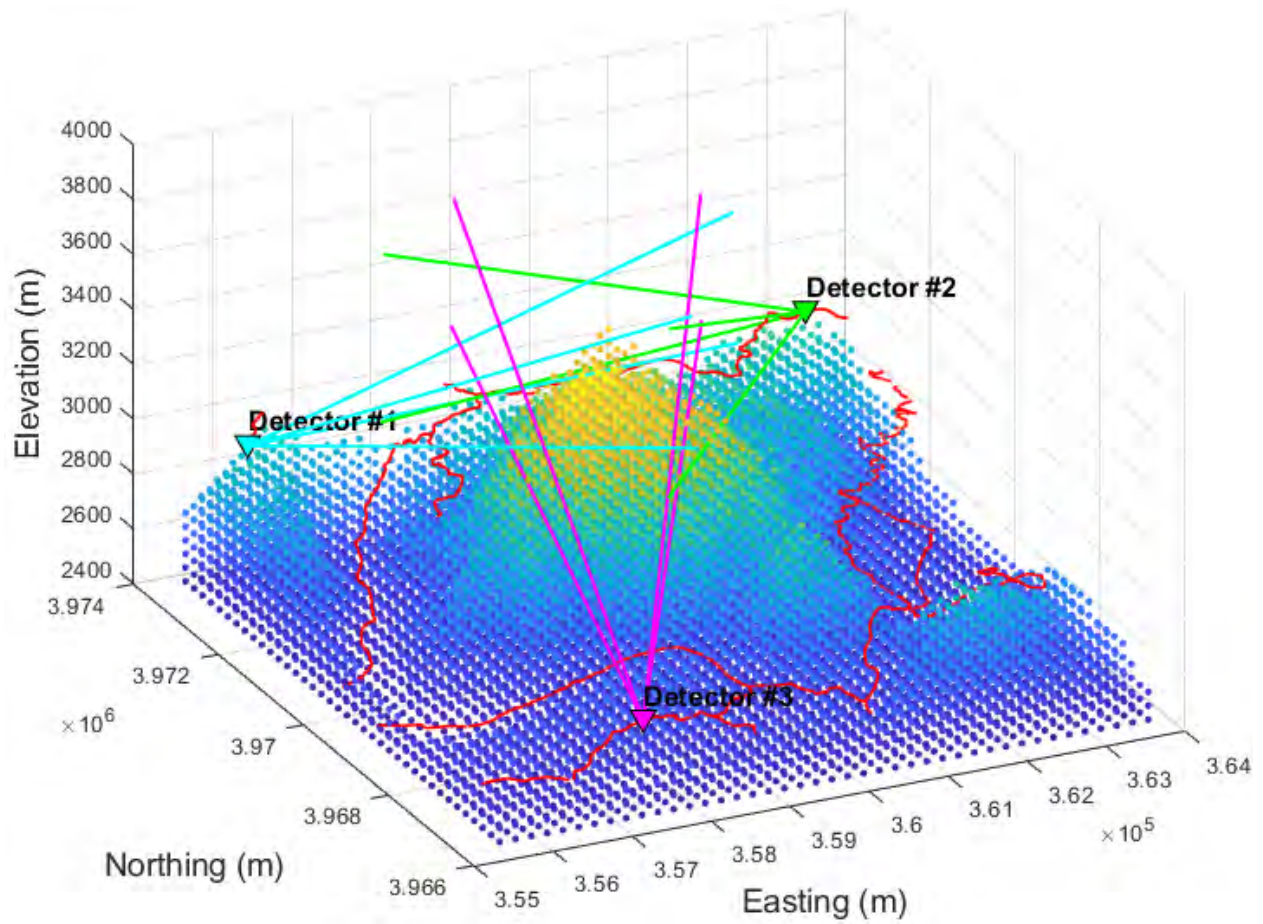


Figure 2: Discretized view of Redondo Peak, composed of uniform prismatic elements of size 200-by-200-by-50 m in the x , y , and z directions respectively. Plotted is the lower left-hand corner of each element. The optimal detector setup with respect to the path length of the central trajectory through the rock at a common reference point is shown. The maximum field of view, considered in this study to arbitrarily be $d\phi = 30^\circ$ and $d\theta = 5^\circ$, is also shown for each detector.

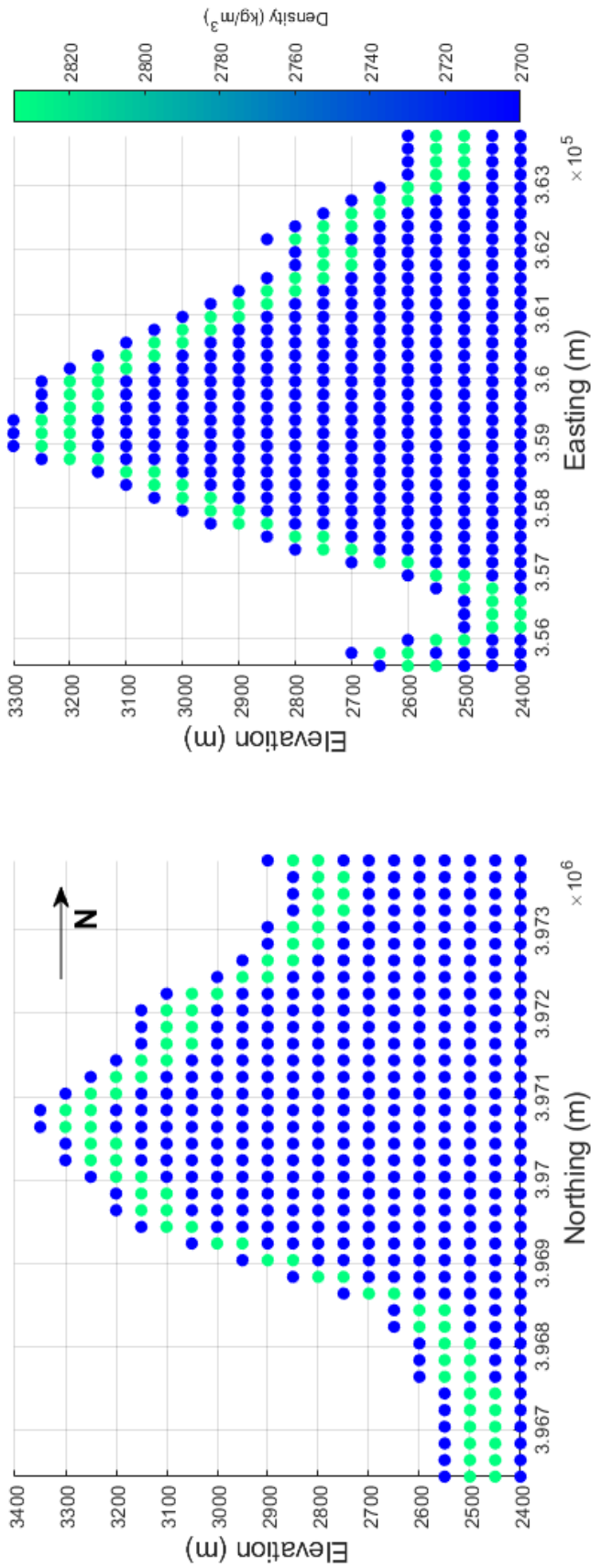
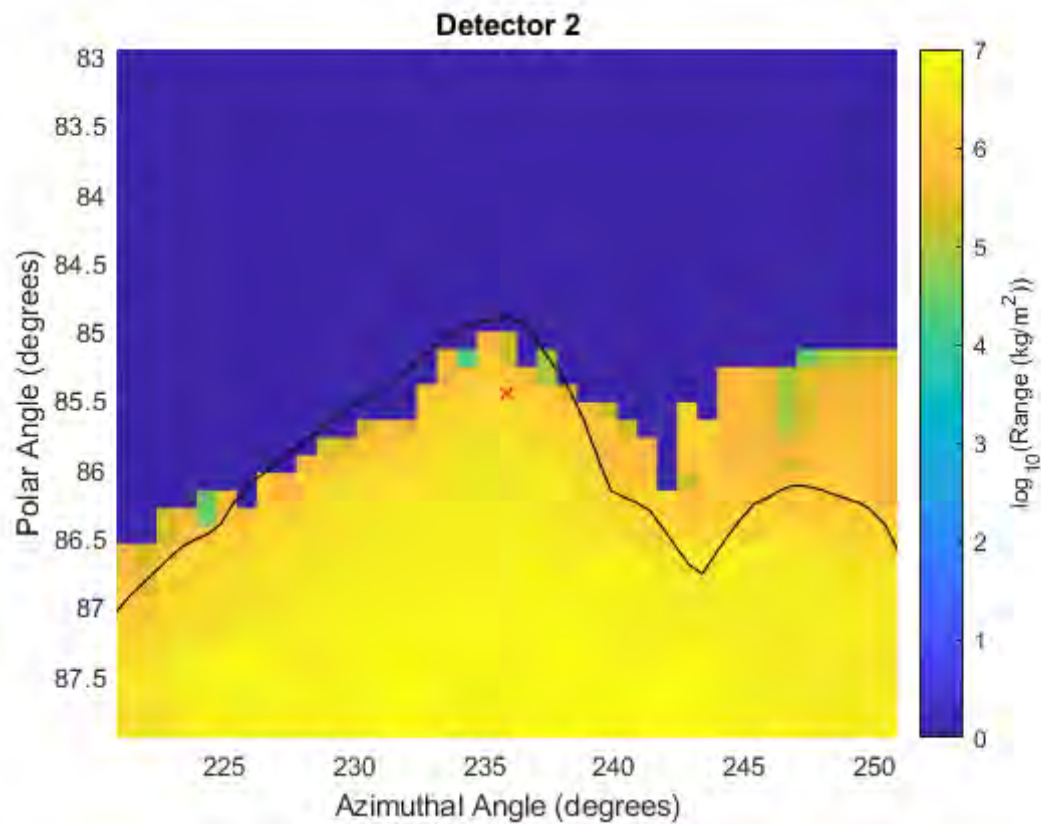
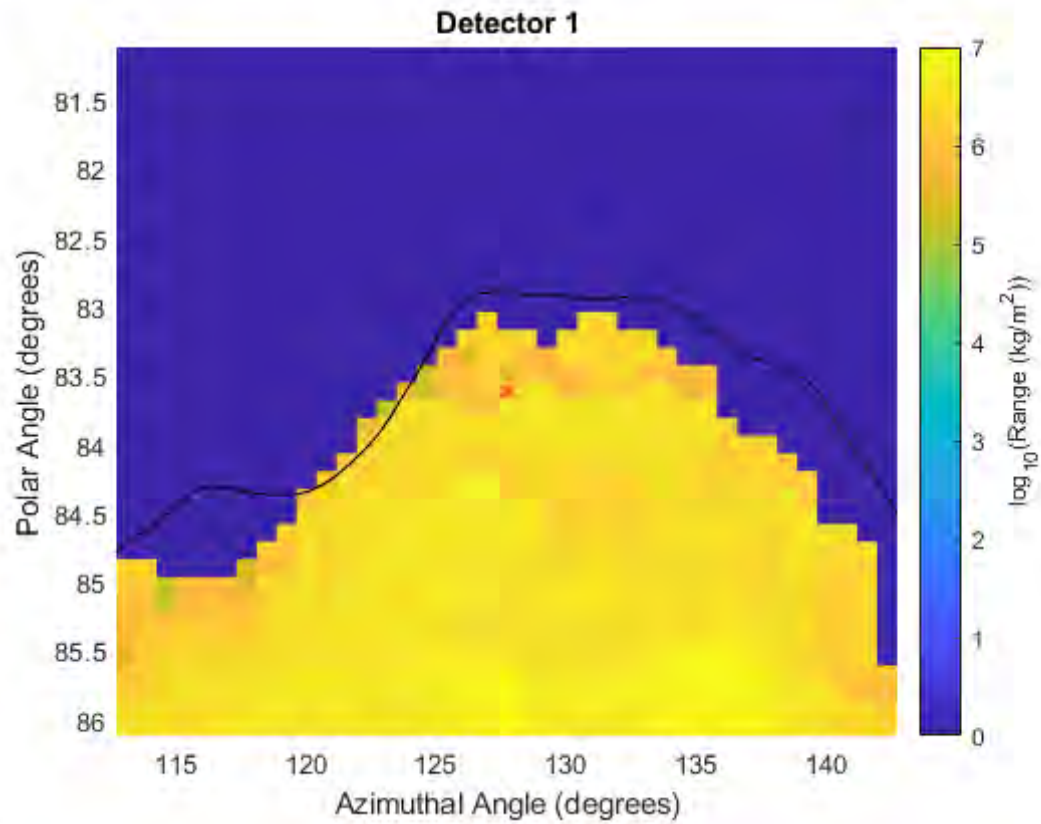


Figure 3: North-South (left) and East-West (right) cross sections through the apex of Redondo Mountain. Plotted are the lower left-hand corners of each prismatic element and their color corresponds to their associated density parameter. There exists a base density of 2700 kg/m³ everywhere except for a 100 m thick table of density 2835 kg/m³ at depth of 50 m below the topographic surface. This perturbed density structure is intended to roughly model a hydrologic signal, like a water table that conforms to the topography of the overlying rock. We intend to synergistically use muon and gravity measurements to resolve this structure.



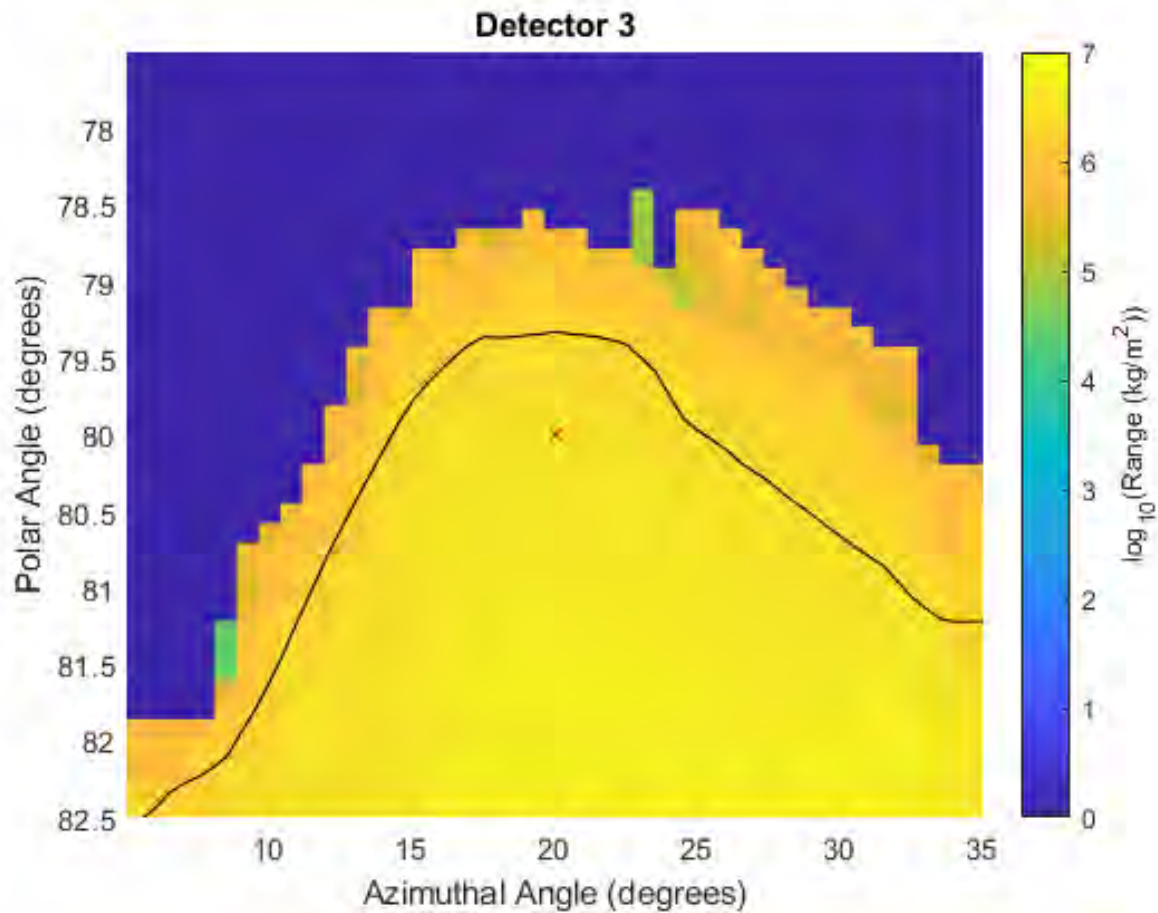


Figure 4: Range values in logarithmic scale, as seen by each of the three detectors. Range values at each of the 1600 trajectories per detector are simply the path length of the trajectory through an individual element multiplied by the element's associated density, and summed over every element that the trajectory traverses within the model. Also plotted in black atop the range colormesh is the projected profile of the maximum elevation from the perspective of each respective detector.

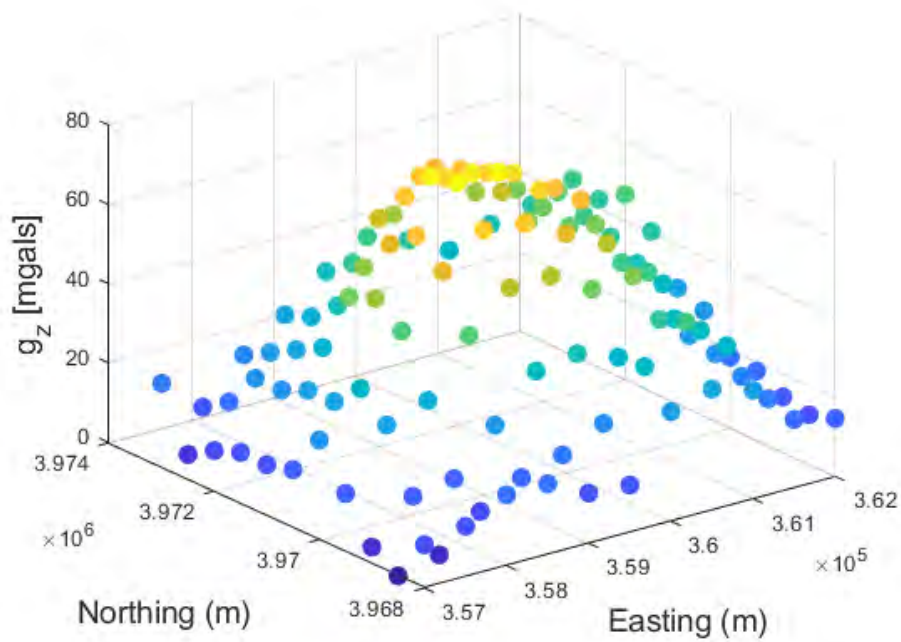
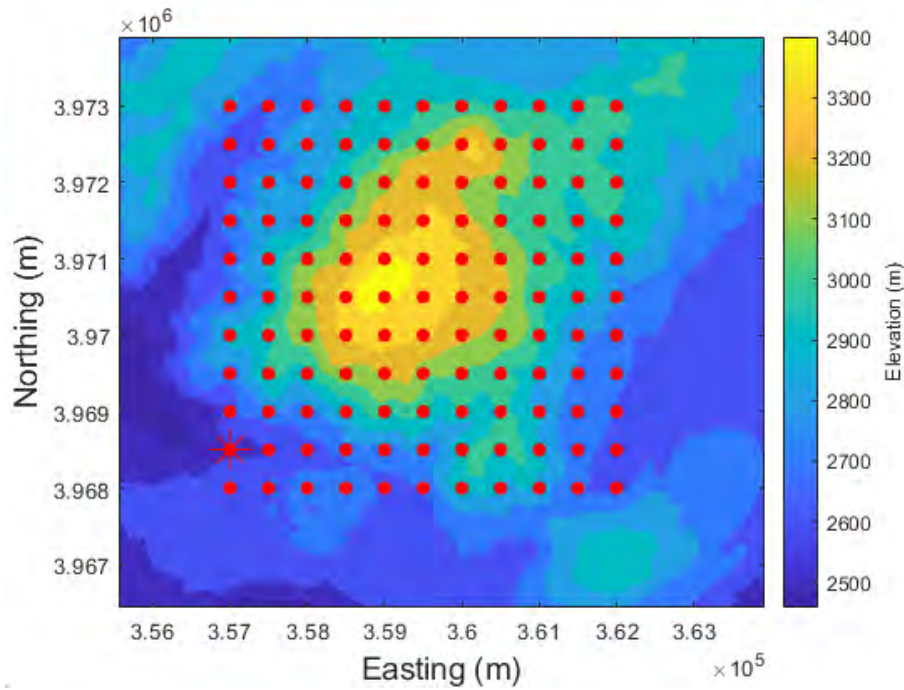


Figure 5: (Top) Locations of 121 gravity stations plotted as red circles. The colormap in this figure is a function of the elevation. (Bottom) Synthetically-generated, relative gravity measurements at each station, shown in mgals. Any relative change in gravity between two stations is purely due to the difference in elevation and the density distribution of elements within the model, and we do not consider extraneous effects that may propagate in a field study, like the Bouguer or Free-Air anomalies. The colormap in this figure is a function of the relative gravity, g_z .

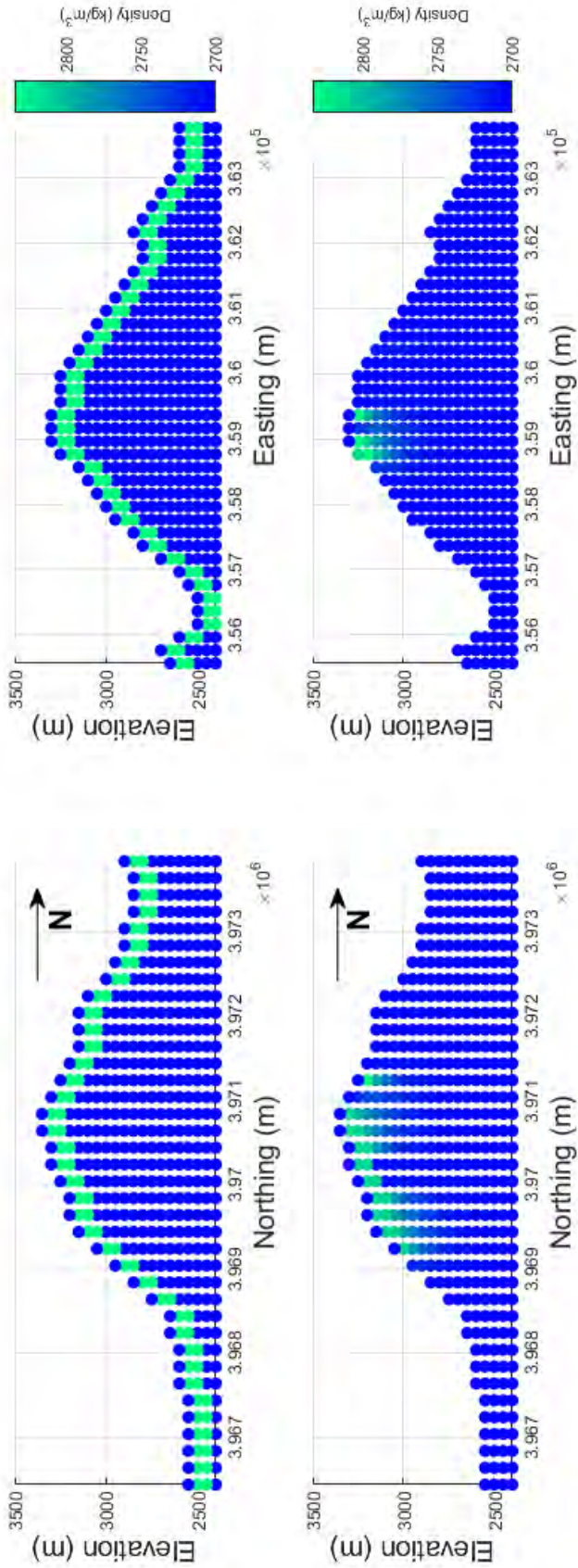


Figure 6: North-South and East-West trending cross section plots centered on Redondo Peak in the forward model (top), and the inverse-reconstructed model (bottom). In those elements of the model constrained by muon measurements, the structure is roughly reconstructed in the inversion, however in those locations not constrained, gravity acts as a singular dataset and subsequently produces an inaccurate result that is inherently due to the nonunique behavior of gravity as a singular dataset. Hyperparameters for this inversion result are $\sigma_\rho = 56.89 \text{ kg/m}^3$, $\lambda = 100 \text{ m}$, and $\rho_{base} = 2700 \text{ kg/m}^3$, and were derived from the true forward model values to present a best-case scenario for the inversion result.

Appendix: Investigating other density structures

For purposes of testing the robustness of our inversion scheme, we introduce another density structure into the model: a low-density sphere of radius 400 m at a depth of 50 m below the surface. Using the same perturbation scheme described in subsection A, we decrease the density of model elements by an arbitrary 10% and investigate the inversion results given no prior information other than an assumption of a constant density starting model.

As expected, our inversion scheme resolves the density anomaly accurately (Fig. 7), and because the anomaly exists solely in the area that is constrained by both muon and gravity measurements, its structure is better resolved than the previously-investigated case.

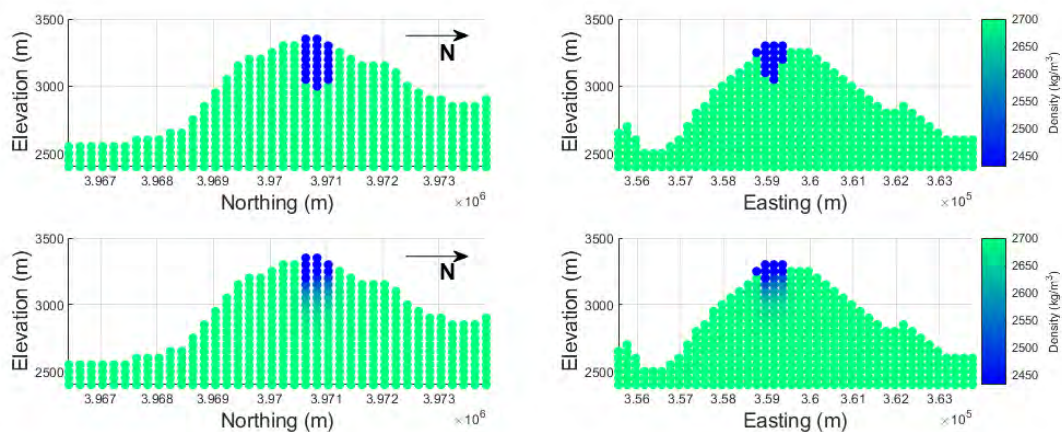


Figure 7: North-South and East-West trending cross section plots centered on Redondo Peak in the forward model (top), and inverse model (bottom). Hyperparameters for this inversion result are $\sigma_\rho = 17.62 \text{ kg/m}^3$, $\lambda = 100 \text{ m}$, and $\rho_{base} = 2700 \text{ kg/m}^3$, and were derived from the true forward model values to present a best-case scenario for the inversion.